



HAL
open science

A Naphthalimide based “Turn-ON” probe for wash-free imaging of lipid-droplet in living cells with an excellent selectivity.

Laurane Michel, Philippe Durand, Arnaud Chevalier

► To cite this version:

Laurane Michel, Philippe Durand, Arnaud Chevalier. A Naphthalimide based “Turn-ON” probe for wash-free imaging of lipid-droplet in living cells with an excellent selectivity.. ChemBioChem, In press, 10.1002/cbic.202400270 . hal-04586962

HAL Id: hal-04586962

<https://hal.science/hal-04586962>

Submitted on 29 May 2024

HAL is a multi-disciplinary open access archive for the deposit and dissemination of scientific research documents, whether they are published or not. The documents may come from teaching and research institutions in France or abroad, or from public or private research centers.

L'archive ouverte pluridisciplinaire **HAL**, est destinée au dépôt et à la diffusion de documents scientifiques de niveau recherche, publiés ou non, émanant des établissements d'enseignement et de recherche français ou étrangers, des laboratoires publics ou privés.

A Naphthalimide based “Turn-ON” probe for wash-free imaging of lipid-droplet in living cells with an excellent selectivity.

Laurane Michel,^[a] Dr. Philippe Durand,^[a] and Dr. Arnaud Chevalier*

[a] Laurane Michel, Dr. Philippe Durand, Dr. Arnaud Chevalier
Université Paris-Saclay, CNRS, UPR 2301
Institut de Chimie des Substances Naturelles, Dpt Chemobiology
91198, Gif-sur-Yvette (France)
E-mail: arnaud.chevalier@cnrs.fr

Supporting information for this article is given via a link at the end of the document.

Abstract: The impacts of dimethylation of 4-Amino-1,8-Naphthalimide (ANI) on its photophysical properties are reported. The resulting 4-DiMe-ANI displays completely different fluorescence properties, conferring it ability to selectively label lipid droplets in living cells. A comprehensive photophysical study revealed that this selectivity arises from an Internal Charge Transfer favored in lipophilic media to the detriment of a non-emissive TICT in more polar media. This results in a very high "LDs/Cytosol" signal ratio, enabling LDs to be imaged with an excellent signal-to-noise ratio, and positioning its performance above that of the BODIPY 493/503 commonly used to image LDs.

Introduction

Lipid droplets (LDs) are part of cellular sub-compartments also called organelles. They feature a hydrophobic core incorporating neutral lipids, surrounded by a layer of phospholipids.^[1] Their main role consists in storing lipids, mainly in their esterified form, such as triacylglycerols, cholesterol or retinyl esters. The proportions of these lipid species in LDs may vary with tissues and their specific storage requirements.^[2] Therefore, LDs regulate the storage and distribution of essential lipids for cell survival. As such, they play a crucial role in cell growth and proliferation. Thus, it is not surprising that LDs dysfunction are associated to fat and overweight-related diseases, such as obesity,^[2] non-alcoholic fatty liver disease,^[3] diabetes^[4] and cardiovascular disorders.^[2] Their role in the development of neurodegenerative diseases^[5] and cancers^[6] as also recently been invoked. Observing LDs is therefore essential to understand their implication in the development of previously mentioned diseases. Among the techniques used in this context, fluorescence microscopy features high sensitivity and allow the observation of living cells. For decades, molecular probes have been developed for LDs imaging by fluorescence microscopy.^[7] The probes generally display a push-pull structure, involving internal charge transfer (ICT) as the fluorescence mechanism. The solvatochromism resulting from the ICT can thus be used to distinguish lipophilic from hydrophilic compartments. Numerous fluorogenic systems, including naphthalimide-based probes,^[8] have evolved from this principle, sometimes permitting ratiometric imaging of LDs.^[9] Turn-ON response to low polarity has also been exploited to observe LDs. A first strategy consists in taking advantage of nonemissive Twisted Intramolecular Charge Transfer Effect (TICT) favored in polar media. The appearance of intense fluorescence can then

arise from a planar conformation of the fluorophore favored in apolar compartments, restoring emissive Internal Charge Transfer (ICT).^[10] Other strategies exploit the viscous nature of LDs. In this case, the use of AIEGens^[11] or molecular rotors^[12] enables OFF-ON sensing of LDs. However, they are sometimes limited by the difficult synthetic access to these complex molecules. In this article, we show how a slight structural modification of a known fluorophore can enable the observation of LDs. Whereas **4-ANI** and its fluorogenic derivatives are widely used in fluorescence imaging,^[13] to our knowledge there are no articles discussing the suitability of its dimethylated analog (**4-DiMe-ANI**). This is probably due to its non-emissive behavior in polar media,^[14] which in this case seems to contraindicate the use of this 4-DiMe-ANI in cellular environments (Figure 1).

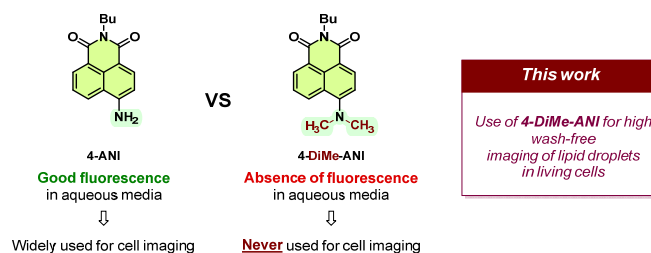


Figure 1. Chemical structures of **4-ANI** and **4-DiMe-ANI**.

This article presents how a simple aniline alkylation of 4-amino-1,8-naphthalimide (**4-ANI**) results in a subcellular redistribution of the fluorescent signal towards LDs, and reveals the reasons for this. The practical utility of 4-dimethylamino-1,8-naphthalimide (**4-DiMe-ANI**) as an environment-sensitive ‘turn-ON’ probe for selective imaging of LDs in living cells is also demonstrated.

Results and Discussion

4-DiMe-ANI targets LDs

This study was motivated by the unexpected subcellular localization of the compound **4-DiMe-ANI** in LDs observed during confocal microscopy experiments (Figure 2a). Whereas **4-ANI** displays a signal predominantly localized in the cytosol with no obvious compartmentalization, the **4-DiMe-ANI**'s fluorescent signal appears to be exclusively located in spherical vesicles similar to lipid droplets (Figure 2a). To confirm this, we carried out a colocalization experiments. The **4-DiMe-ANI** (5 μM) was incubated in the presence of a red lipid droplet marker (LS610®)^[15], in A549 lung cancer living cells.

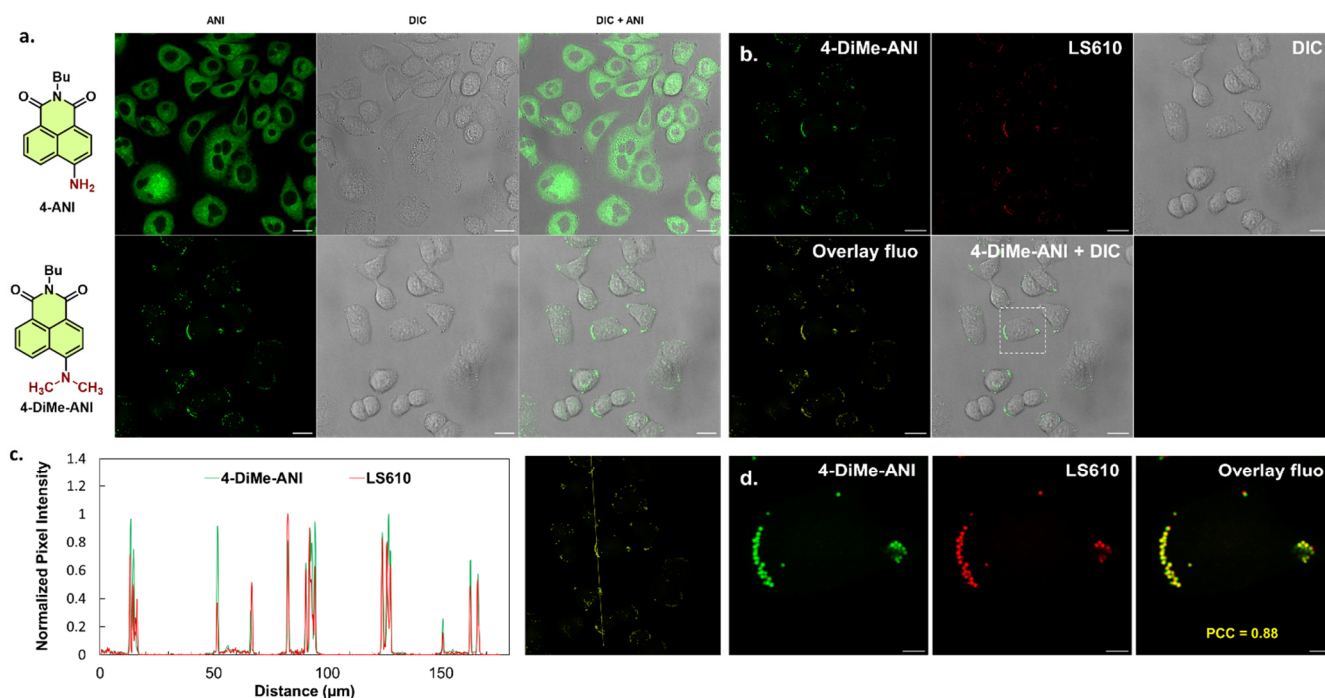


Figure 2. Confocal microscopy reveals the selectivity of 4-DiMe-ANI for lipid droplets. **a.** Imaging of **4-ANI** and **4-DiMe-ANI** using a 63x oil immersion objective, at 5 μM after 3h of incubation at 37 $^{\circ}\text{C}$ (λ_{Exc} : 440 nm, λ_{Em} : 450 to 550 nm). Scale bar 20 μm . **b.** Colocalization experiments. **4-DiMe-ANI** was incubated at 5 μM for 3 h at 37 $^{\circ}\text{C}$, then **LipidSpot 610**[®] was added using procedure suggested by the Biotium company. Scale bar 20 μm . **c.** Plot profile of **4-DiMe-ANI** and **LipidSpot610**[®] recorded using the JAcOP plugin of ImageJ. **d.** Zoomed image of panel b. Scale bar 5 μm . PCC was calculated using JAcOP plugin of ImageJ.

The resulting images (Figure 2b) demonstrated a good correlation between the two signals, materialized by the yellow signal observed on the overlay image. This result was fully consolidated by the plot profile experiment (Figure 2c) and zoomed image (Figure 2d), together revealing a strong correlation between the signals of **4-DiMe-ANI** and **BODIPY 493/503**. The zoomed images presented in Figure 2d confirms the very good colocalization of **4-DiMe-ANI** and **LS610**[®], with a Pearson Correlation Coefficient (PCC) measured at 0.88. Given the movement of lipid droplets in living cells, the overlay of the two fluorescent signals is very complex to achieve. Consequently, the PCC value is in this case most likely underestimated and should be considered with caution. Altogether, these results confirm the ability of **4-DiMe-ANI** to target LDs, making it a good candidate as a fluorescent marker for these organelles.

Rationalisation by photophysical study

To better understand the apparent selectivity of **4-DiMe-ANI** for LDs, we undertook a comprehensive study of its photophysical properties starting with a solvatochromism study. The absorption and emission spectra of the fluorophore were measured in various solvents over a wide range of polarity (Fig. S1). Molar absorption coefficients and fluorescence quantum yields were calculated and reported in Table of Figure 3. The **4-DiMe-ANI** has a fairly constant solvent-dependent absorption maximum centered between 404 and 426 nm. By contrast, the effect of solvent polarity on emission properties is much more visible. The emission of **4-DiMe-ANI** increases from 500 nm in the lowest-polarity solvent (toluene) to 549 nm in DMSO, i.e. a bathochromic shift of 49 nm. This feature is in line with the “push-pull” nature of this fluorophore.

Solvent	λ_{max} abs (nm) ^a	ϵ_{max} ($\text{M}^{-1} \text{cm}^{-1}$)	λ_{max} Em (nm)	Stokes shift (cm^{-1})	QY_{Fl} ^b
Toluene	404	17 600	500	4 752	0.98
CHCl_3	414	19 500	505	4 353	0.95
CH_2Cl_2	412	19 400	511	4 702	0.94
Triacetin	412	16 800	519	5 004	0.32
THF	408	17 900	513	5 017	0.42
CH_3CN	416	19 100	530	5 171	0.04
Acetone	413	18 700	530	5 345	0.04
DMSO	426	15 800	549	5 259	<0.01
EtOH	424	21 500	537	4 963	0.01
MeOH	423	18 800	547	5 359	<0.01
PBS 1X	440	12 300	553	4 752	<0.01

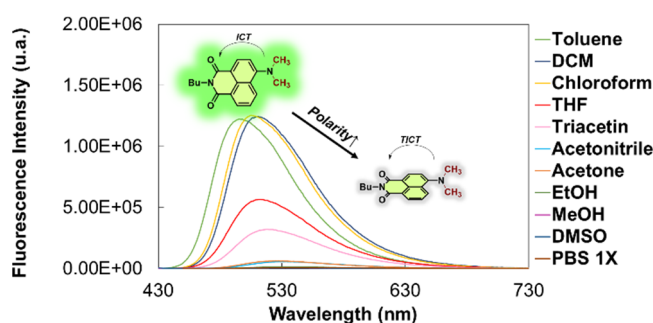


Figure 3. Solvatochromism study for 4-DiMe-ANI. **Left.** Table of photophysical properties of **4-DiMe-ANI**, ^aAbsorbance maxima were measured at the S₀→S₁ transition, ^brelative fluorescence QY were determined at 25 $^{\circ}\text{C}$ using coumarin 153 as reference ($\text{QY}_{\text{Fl}} = 0.53$ in EtOH)^[16]. **Right.** Overlap of emission spectra of **4-DiMe-ANI**, in different solvents measured for an absorbance value of 0.05 and recorded at 25 $^{\circ}\text{C}$ between 430 and 730 nm.

The key finding from this study concerns the impact of solvent polarity on its fluorescence efficiency. Indeed, excellent fluorescence quantum yields (QY_{FI}) were determined in apolar solvents such as toluene (0.98) or in chlorinated solvents such as chloroform (0.95) and dichloromethane (0.94). On the other hand, an increase in polarity, even moderate, rapidly causes a drop in QY_{FI} . It is only 0.04 in aprotic polar solvents such as acetone or acetonitrile, and approaches complete absence of fluorescence in protic polar solvents such as ethanol, methanol or PBS buffer. This major difference between polar and apolar media may partly explain the selective observation of **4-DiMe-ANI** in lipophilic cell compartments, in this case lipid droplets. We then further studied

the influence of aggregation on the emission properties of **4-DiMe-ANI**. Emission spectra of 10 μM solution of **4-DiMe-ANI** were acquired in THF, with increasing amounts of H_2O to promote fluorophore aggregation. An intense fluorescence ($QY_{FI} = 0.42$) was observed in THF (Figure 4a), which decreases significantly as soon as the percentage of water increases. A slight increase was observed from 80% to 90% of water while precipitation occurred in water. The latter increase in fluorescence is not significant enough to consider **4-DiMe-ANI** as an efficient AIEGen dye. Therefore, we can exclude aggregation's involvement in the fluorescence enhancement mechanism of **4-DiMe-ANI** in LDs.

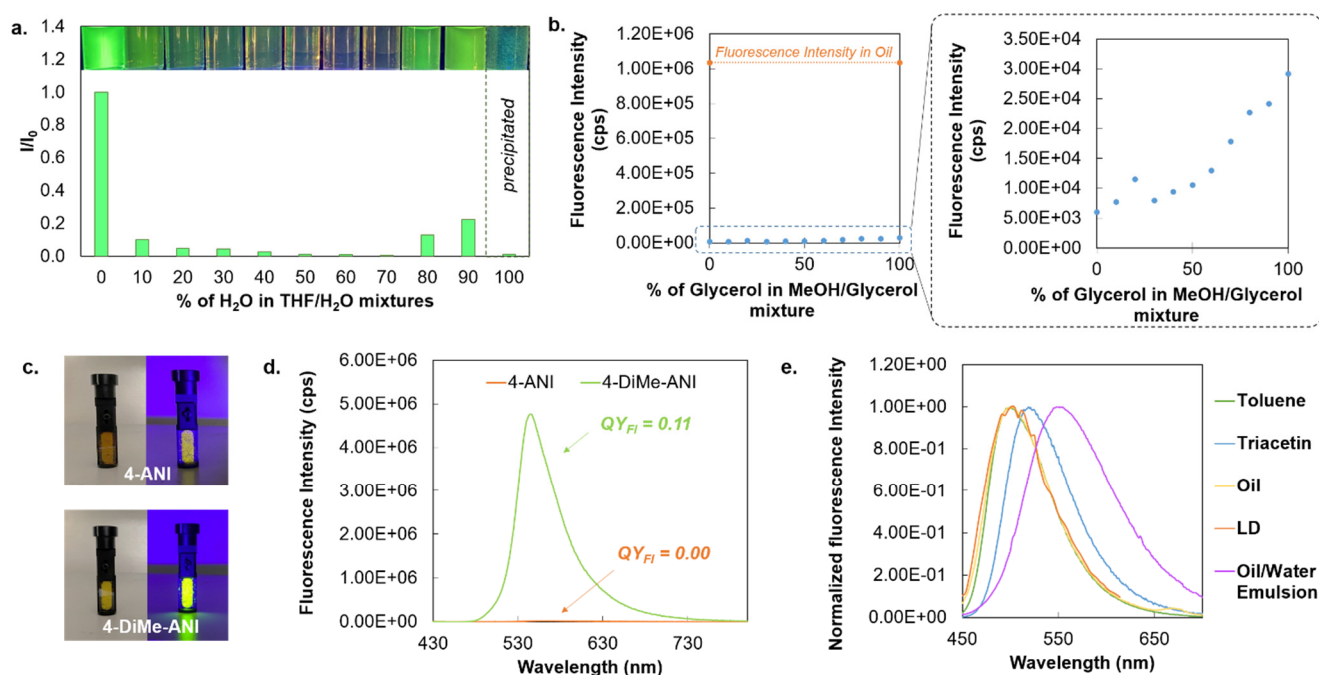


Figure 4. a. Fluorescence Intensity of **4-DiMe-ANI** in solution at 10^{-5} M in different THF/ H_2O mixtures with different percentage of H_2O , normalized to the maximum THF sample Intensity (λ_{Exc} : 410 nm). Photography of the **4-DiMe-ANI** 10^{-5} M solutions under illumination at 365 nm b. Study of viscosity impact illustrated by the fluorescence Intensity of **4-DiMe-ANI** in solution at 10^{-5} M in different MeOH/Glycerol mixtures with different percentage of Glycerol (λ_{Exc} : 410 nm, λ_{Em} : 540 nm) c. Photography of **4-ANI** and **4-DiMe-ANI** powders with or without illumination at 365 nm d. Emission spectra and fluorescence quantum yields of **4-ANI** and **4-DiMe-ANI** in solid state. e. Normalized emission spectra of **4-DiMe-ANI** in different media including lipid droplets (λ_{Exc} : 410 nm for Toluene, triacetin, canola oil and W/O emulsion, λ_{Exc} : 440 for LDs).

We then performed measurements in different MeOH/Glycerol mixtures to study the influence of viscosity on the fluorescence of **4-DiMe-ANI** (Figure 4b). While a slight increase in fluorescence was observed with viscosity its magnitude cannot justify the strong fluorescence signal generated by **4-DiMe-ANI** in LDs. Finally, we measured fluorescence in the solid state and compared it with that of **4-ANI** (Figure 4c-d). **4-DiMe-ANI** shows quite good fluorescence fluorescence ($QY_{FI} = 0.11$, See Figure. S2). This result could be explained by the restriction of the C-N bond rotation that prevents, at least in part, the formation of a non-emissive twisted form. In the meantime, unsubstituted **4-ANI** for which the rotation or the C-N bond is easier did not display any significant fluorescent signal (Figure. S2). We measured the emission spectrum of **4-DiMe-ANI** in LDs using a confocal microscope (Figure 4e) and superposed it to those recorded in toluene, canola oil, triacetin, or in a Water/Oil emulsion reported as possible mimics for LD's environment.^[17] Both Triacetin and Oil/Water emulsion revealed results significantly in contrast with spectral measurements carried out within the LD. This suggests

that they do not constitute, in our case, a relevant model of the LD environment for the study of the photophysical properties of **4-DiMe-ANI**. The excellent correspondence between the intra-LDs spectra and the spectra in canola oil and toluene suggests a significant contribution of the apolarity in the appearance of the intense fluorescent signal in LDs. This set of data demonstrates that **4-DiMe-ANI** exhibits a Turn-ON response to the intra-LD environment. This exaltation can be attributed to the prevalence of a planar conformation, allowing a highly emissive ICT in apolar media, to the detriment of a non-emissive twisted conformation (TICT) present in more polar media (Figure 3, right). This OFF/ON behavior constitutes a considerable benefit for contrast enhancement in cell imaging experiments, thanks to an improved signal-to-noise ratio.

4-DiMe-ANI as an alternative to BODIPY 493/503

To highlight the performances of **4-DiMe-ANI**, we compared it with **BODIPY 493/503** (Figure 5a), a commercially available green marker^[18] commonly used for LD labeling.^[19] First, we

assessed the photobleaching resistance of the two fluorophores. Under continuous irradiation at a power of $40 \text{ mW}\cdot\text{cm}^{-2}$, a 75% decrease in the **BODIPY 493/503** fluorescence signal was observed after 2h of illumination (Figure 5b-c). On the other hand, 80% of the signal emitted by **4-DiMe-ANI** was retained after 2h of irradiation under the same conditions, attesting to its greater resistance to photobleaching. We also conducted a confocal microscopy study to quantify the “LD/Cytosol” signal ratio of the two fluorophores. (Figure 5d). For this purpose, we measured the fluorescence signal intensity inside ten different LDs and ten different areas in the cytosol (Figure. S3). We then calculated the average “LDs/Cytosol” signal values (Figure 5d-e). The fluorescence signal appears 18.7 and 7.6 times more intense in LDs than in the cytosol for **4-DiMe-ANI** and **BODIPY 493/503**, respectively.

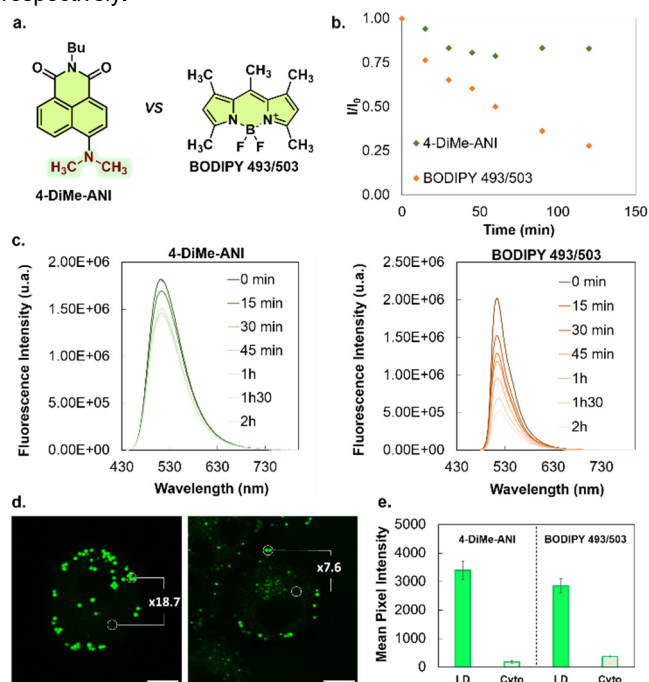


Figure 5. Comparison of LD selectivity between 4-DiMe-ANI and BODIPY 493/503. a. Chemical structures of **4-DiMe-ANI** and **BODIPY 493/503**. b. Comparison of fluorescence intensity decreases over the time after irradiation at 470 nm ($40 \text{ mW}\cdot\text{cm}^{-2}$) for **4-DiMe-ANI** (green) and of **BODIPY 493/503** (in orange). c. Overlap of the fluorescence spectra of **4-DiMe-ANI** (left) and **BODIPY 493/503** (right) in toluene at 25°C periodically recorded during a 2 h of period of irradiation at 470 nm ($40 \text{ mW}\cdot\text{cm}^{-2}$). d. Imaging of **4-DiMe-ANI** (λ_{Exc} : 440 nm, λ_{Em} : 450 to 550 nm) and **BODIPY 493/503** (λ_{Exc} : 490 nm, λ_{Em} : 500 to 600 nm) using a 63x oil immersion objective, at $5\mu\text{M}$ after 3h of incubation at 37°C . Scale bar $5\mu\text{m}$. e. fluorescence intensity measured in cells with average values calculated with $n = 10$ measurements.

This result highlights the higher selectivity of **4-DiMe-ANI** than **BODIPY 493/503** for LDs. This may be assigned to the efficient Turn-ON response of **4-DiMe-ANI** observed inside the LDs environment. Finally, we assessed cell viability in the presence of both probes. **4-DiMe-ANI** was found to be slightly more cytotoxic upon 72 h of incubation (Figure. S4). However this did not compromise its use at $5\mu\text{M}$ for cell imaging experiments. The efficient OFF-ON response of **4-DiMe-ANI** to the apolar environment suggests a potential use for this probe without recourse to washing steps.

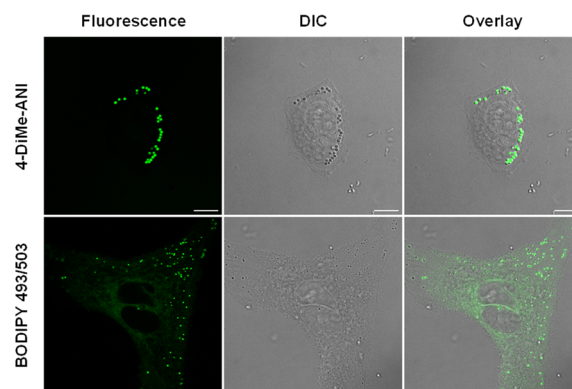


Figure 6. Wash-free Imaging of **4-DiMe-ANI** (λ_{Exc} : 440 nm, λ_{Em} : 450 to 550 nm) and **BODIPY 493/503** (λ_{Exc} : 490 nm, λ_{Em} : 500 to 600 nm) using a 63x oil immersion objective, at $5\mu\text{M}$. Images were recorded after 1h of incubation at 37°C . Scale bar $10\mu\text{m}$.

To confirm this, A549 cells were cultured in the presence of a $5\mu\text{M}$ solution of **4-DiMe-ANI** for 30 min. We then proceeded directly to the microscopy experiments, without any prior washing step. The images revealed remarkably good contrast, validating the use of **4-DiMe-ANI** for wash-free imaging of lipid droplets in living cells (Figure 6). Note that the same experiment carried out with **BODIPY 493/503** also allows the observation of LDs, but with clearly lower selectivity.

Conclusion

To conclude, this study demonstrates the use of **4-DiMe-ANI** as “Turn-ON” probe for selective wash-free imaging lipid droplets in living cells using confocal microscopy experiments. A complete photophysical study was performed and provided a rationalization of this behavior. **4-DiMe-ANI** emerges as a serious candidate for regular use in lipid droplet imaging and outperformed **BODIPY493/503**, a commercial marker commonly used in this field. In top of demonstrating the performance of **4-DiMe-ANI**, this work highlights the impact that minor structural changes in fluorophores can have, both from a photophysical point of view and in terms of sub cellular compartment selective imaging.

Experimental Section

Material

Unless otherwise noted, all commercially available reagents and solvents were used without further purification. TLC were carried out on silica gel aluminum plates with F-254 indicator; Spots were directly visualized or through illumination with UV lamp ($\lambda = 254/365 \text{ nm}$). Flash-column chromatography purifications were performed on silica gel ($40\text{--}63\mu\text{m}$) from Interchim. Organic solvents for spectroscopy were purchased from Acros Organics or Sigma Aldrich. Absolute EtOH was provided by Carlo Erba. The HPLC grade MeCN used for RP-HPLC analyses was obtained from Carlo Erba. Formic acid (FA, puriss p.a., ACS reagent, reagent grade, $\geq 98\%$) was provided by Merck-Millipore (brand Sigma-Aldrich). Aq. mobile-phases for HPLC were prepared using water purified with a Milli-Q Integral 3 system from Merck-Millipore (purified to $18.2 \text{ MW}\cdot\text{cm}$). RPMI 1640 (1X), DPBS (1X), used for cell culture were purchased from Life technologies. LipidSpot™ 610 were purchased from Biotium.

Instrument and methods

¹H NMR spectra were recorded on a Bruker Avance 500 or 300 MHz and proton-decoupled carbon ¹³C NMR spectra were recorded at 126 MHz. NMR experiments were carried out in appropriate deuterated solvent and chemical shifts are expressed in parts per million (ppm) from the residual nondeuterated solvent signal. Calibration was made by using residual signals of partially deuterated solvent summarized in 2010 by Fulmer et al.^[20] The following abbreviations are used for the multiplicities: s: singlet; d: doublet; t: triplet; q: quadruplet; qt: quintuplet; m: multiplet or overlap of nonequivalent resonances; brs: broad singlet; Coupling constants (*J*) are reported in hertz (Hz). High-resolution mass spectra were determined on an AEI MS-9 using electrospray ionization (ESI) and a time-of-flight (TOF) analyzer

Synthesis of 4-DiMe-ANI

6-(dimethylamino)-1H,3H-benzo[de]isochromene-1,3-dione

The compound was synthesized using a method adapted from the literature.^[21] A suspension of 4-bromo-1,8-naphthalic anhydride (2.00 g, 7.25 mmol, 1.00 eq.), dimethylamine hydrochloride (4.73 g, 57.9 mmol, 8.00 eq.), and CuSO₄·5H₂O (181 mg, 0.725 mmol, 0.10 eq.) in DMF (30 mL), triethylamine was added (10.2 mL, 72.5 mmol, 10.0 eq.), and the mixture was then refluxed while heating for 3 h. The solution was concentrated in vacuo to remove the DMF, and the residue was crystallized from MeOH to obtain the product as a yellow solid (1.66 g, 95 %). Analyses were in accordance with the literature. ¹H NMR (500 MHz, CDCl₃) δ 8.49 (d, *J* = 7.3 Hz, 1H), 8.46 (d, *J* = 8.5 Hz, 1H), 8.37 (d, *J* = 8.3 Hz, 1H), 7.64 (t, *J* = 7.6 Hz, 1H), 7.06 (d, *J* = 8.3 Hz, 1H), 3.18 (s, 6H). HRMS calculated for C₁₄H₁₂NO₃ [M+H]⁺ 242.0817, found 242.0815.

4-DiMe-ANI

The 6-(dimethylamino)-1H,3H-benzo[de]isochromene-1,3-dione (200 mg, 0.829 mmol, 1.00 eq) and *n*-butylamine (164 μL, 1.66 mmol, 2.00 eq.) were refluxed in EtOH (0.10 M) overnight. Solvents were evaporated and resulting residue was dissolved in 20.0 mL of DCM. The organic phase was washed with a NH₄Cl saturated aqueous solution (3 x 20 mL). Organic phase was dried over MgSO₄ and solvents were evaporated under reduced pressure. The crude product was purified by flash chromatography on silica gel (Hept/EA, 100/0 to 90/10, v/v) to afford product (139.2 mg, 57%) as a yellow solid. ¹H NMR (500 MHz, MeOD) δ 8.39 (d, *J* = 8.2, 0.8 Hz, 1H), 8.35 (dd, *J* = 7.3, 0.8 Hz, 1H), 8.25 (d, *J* = 8.3 Hz, 1H), 7.59 (t, *J* = 7.4 Hz, 1H), 7.08 (d, *J* = 8.3 Hz, 1H), 4.03 (t, *J* = 7.5 Hz, 2H), 3.08 (s, 6H), 1.62 (qt, *J* = 7.5 Hz, 2H), 1.40 (sx, *J* = 7.4 Hz, 2H), 0.97 (t, *J* = 7.4 Hz, 3H) ppm. ¹³C NMR (125 MHz, MeOD) δ 14.1, 21.3, 31.3, 40.9, 45.0, 114.2, 115.1, 123.8, 125.8, 126.2, 131.3, 131.9, 132.8, 133.7, 158.6, 165.4, 165.9 ppm. HRMS calculated for C₁₈H₂₁N₂O₂ [M+H]⁺ 297.1603, found 297.1594. ¹H NMR and HRMS spectra are accessible in the SI file (Fig. S5 and S6)

Spectroscopy

UV-Visible absorption spectra were recorded on a Varian Cary 100 Series 2 Scan UV-Vis Spectrophotometer using a 10 mm path quartz cell. Emission spectra experiments were performed on an Edinburgh FS-5 spectrofluorimeter with a SC-20 module. Aright angle configuration was used. The relative fluorescence quantum yields were determined using coumarin 153 as

reference (φ_{FL} = 0.58 in EtOH) as reference with the following formula:

$$QY_{FI}(x) = S_x/S_s(n_x/n_s)^2 \cdot QY_{FI}(s)$$

Where *S* is the slope of the linear plot of the integrated fluorescence intensity in function of the absorbance value, *n* is the refractive index of the solvents (at 25 °C) used in measurements, and the subscripts *s* and *x* represent standard and unknown, respectively.

Cell culture

A549 lung cancer cells. Human cancer cell lines were obtained from the American type Culture Collection (ATCC, Rockville, USA) and were cultured according to the supplier's instructions. A549 lung carcinoma cells were grown in RPMI 1640 containing 10% FCS and 1% glutamine. All cell lines were maintained at 37 °C in a humidified atmosphere containing 5% CO₂. For live cells fluorescence microscopy, an Ibidi® μSlide 8 Well high Glass Bottom plate was seeded with 20 000 cells/well and then maintained at 37 °C in a humidified atmosphere containing 5% CO₂ for 24h to 48h.

Confocal microscopy

After adequate confluence was obtained in Ibidi® μSlide 8 Well high Glass Bottom plate, the medium was removed and replaced by a solution of fluorophore at the desired concentration in the appropriate medium, prepared from a stock solution of fluorophore in DMSO (concentration of DMSO was kept under 1% v/v). The dye in incubated for 1 h or longer, after what the sample is ready for imaging. No wash is needed. For Co-localisation experiments: after incubation with **4-DiMe-ANI**, the medium was removed, washed once with PBS buffer and a 1X of LipidSpot™ 610 solution in appropriate medium was then added. The cells were incubated for 15 minutes at 37 °C, after what the medium was removed, cells were washed once with warmed PBS (1X) then appropriate fresh medium was added before imaging. Fluorescence images were acquired using a Leica SP8-X inverted confocal microscope with a 63× oil immersion objective (HC PL APO CS2 Leica). Excitation was performed using a White light laser pulsed at 80 MHz and a Diode 440 nm LDH-P-C-440B pulsed at 40 MHz. Detection was carried out by using PMT detector (Hamamatsu 6357) collecting photons, or GaAsP Hybrid (Hamamatsu) collecting photons over the appropriate emission wavelength window.

Acknowledgements

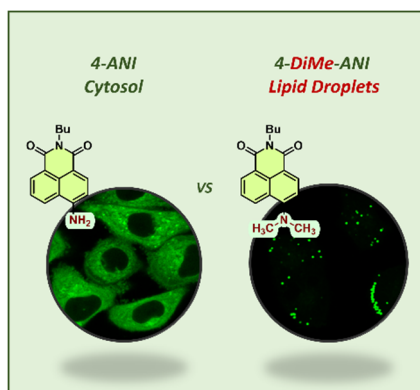
This project has received funding by the French National Research Agency under the program ANR-21-CE18-0005-01 grant. This work has also been supported as part of France 2030 programme "ANR-11-IDEX-0003". We also thank the Institut de Chimie des Substances Naturelles for their financial support. The present work has benefited from the Imagerie-Gif light microscopy core facility supported by the French National Research Agency (ANR-11-EQPX-0029/Morphoscope, ANR-10-INBS-04/FranceBioImaging; ANR-11-IDEX-0003-02/Saclay Plant Sciences). Lilian Estaque is acknowledged for solid-state

fluorescence QY measurements. Université Paris-Saclay and the CNRS are also acknowledged.

Keywords: Fluorophore • Lipid Droplet • Polarity • Cell Imaging • Naphthalimide

- [1] Y. Jin, Y. Tan, J. Wu, Z. Ren, *Cell Death Dis.* **2023**, *9*, 254.
- [2] A. Zadoorian, X. Du, H. Yang, *Nat. Rev. Endocrinol.* **2023**, *19*, 443-459.
- [3] E. Scorletti, R. M. Carr, *J. Hepatol.* **2022**, *76*, 934-945.
- [4] M. Konige, H. Wang, C. Sztalryd, *Biochim. Biophys. Acta* **2014**, *1842*, 393-401.
- [5] Z. Q. Lan, Z. Y. Ge, S. K. Lv, B. Zhao, C. X. Li, *Cell Death Dis.* **2023**, *9*, 229.
- [6] aA. L. S. Cruz, E. A. Barreto, N. P. B. Fazolini, J. P. B. Viola, P. T. Bozza, *Cell Death Dis.* **2020**, *11*, 105; bD. Delmas, A. K. Cotte, J. L. Connat, F. Hermetet, F. Bouyer, V. Aires, *Cancers* **2023**, *15*; cT. Petan, *Rev. Physiol. Biochem. Pharmacol.* **2023**, *185*, 53-86.
- [7] aH. Tian, A. C. Sedgwick, H.-H. Han, S. Sen, G.-R. Chen, Y. Zang, J. L. Sessler, T. D. James, J. Li, X.-P. He, *Coord. Chem. Rev.* **2021**, *427*, 213577; bT. K. Fam, A. S. Klymchenko, M. Collot, *Materials* **2018**, *11*; cY. Zhao, W. Shi, X. Li, H. Ma, *Chem. Commun.* **2022**, *58*, 1495-1509.
- [8] aX. Zheng, W. Zhu, F. Ni, H. Ai, S. Gong, X. Zhou, Jonathan L. Sessler, C. Yang, *Chem. Sci.* **2019**, *10*, 2342-2348; bJ.-Y. Ni, X.-F. Weng, R. Sun, Y.-J. Xu, J.-F. Ge, *Dyes Pigm.* **2021**, *186*, 109003; cX. Li, J. Bian, M. Fu, Y. Zhang, H. Liu, B. Gao, *Anal. Methods* **2022**, *14*, 1279-1284; dI. R. D. Johnson, E. E. Rudebeck, M. J. Sweetman, A. Sorvina, T. D. Ashton, F. M. Pfeffer, D. A. Brooks, S. M. Hickey, *Sens. Actuator B-Chem.* **2022**, *365*, 131921; eS. M. Hickey, I. R. D. Johnson, E. Dallerba, M. J. Hackett, M. Massi, J. Lazniewska, L. A. Thurgood, F. M. Pfeffer, D. A. Brooks, T. D. Ashton, *Dyes Pigm.* **2023**, *217*, 111382.
- [9] aA. H. Ashoka, P. Ashokkumar, Y. P. Kovtun, A. S. Klymchenko, *J. Phys. Chem. Lett.* **2019**, *10*, 2414-2421; bJ. Valanciunaite, E. Kempf, H. Seki, D. I. Danylchuk, N. Peyrieras, Y. Niko, A. S. Klymchenko, *Anal. Chem.* **2020**, *92*, 6512-6520; cM. Collot, S. Bou, T. K. Fam, L. Richert, Y. Mély, L. Danglot, A. S. Klymchenko, *Anal. Chem.* **2019**, *91*, 1928-1935.
- [10] aS. Pei, J. Li, C. Zhang, G. Zhang, Y. Zhou, L. Fan, W. Wang, S. Shuang, C. Dong, *ACS Biomater. Sci. Eng.* **2022**, *8*, 253-260; bY. Li, M. Zhang, X. Chen, J. Liang, D. Chen, M. Gao, L. Ren, *Tetrahedron Lett.* **2019**, *60*, 1880-1884; cC. J. Wu, X. Y. Li, T. Zhu, M. Zhao, Z. Song, S. Li, G. G. Shan, G. Niu, *Anal. Chem.* **2022**, *94*, 3881-3887.
- [11] aE. Tacke, M. D. Hoang, L. Estaque, P. Durand, G. Pieters, A. Chevalier, *Org. Biomol. Chem.* **2024**; bE. Tacke, M.-D. Hoang, K. Tatoueix, B. Keromnes, E. Van Eslande, P. Durand, G. Pieters, A. Chevalier, *Chem. Sci.* **2023**, *14*, 6000-6010; cF. Zhang, X. Wu, B. Liu, T. Han, D. Yan, D. Wang, B. Zhong Tang, *Coord. Chem. Rev.* **2023**, *493*, 215337; dL. Wang, X. Chen, X. Ran, H. Tang, D. Cao, *Dyes Pigm.* **2022**, *203*, 110332.
- [12] aT. Mukherjee, R. J. Martinez-Sanchez, K. T. Fam, S. Bou, L. Richert, D. Garnier, Y. Mély, S. Kanvah, A. S. Klymchenko, M. Collot, *Mater. Chem. Front.* **2021**, *5*, 2459-2469; bB. Dong, W. Song, Y. Lu, Y. Sun, W. Lin, *ACS Sens.* **2021**, *6*, 22-26; cC. W. Song, U. Tamima, Y. J. Reo, M. Dai, S. Sarkar, K. H. Ahn, *Dyes Pigm.* **2019**, *171*, 107718.
- [13] aC. Geraghty, C. Wynne, R. B. P. Elmes, *Coord. Chem. Rev.* **2021**, *437*, 213713; bN. Jain, N. Kaur, *Coord. Chem. Rev.* **2022**, *459*, 214454; cL. Michel, M. Auvray, L. Askenatzis, M.-A. Badet-Denisot, J. Bignon, P. Durand, F. Mahuteau-Betzer, A. Chevalier, *Anal. Chem.* **2024**, *96*, 1774-1780.
- [14] aS. Saha, A. Samanta, *J. Phys. Chem. A* **2002**, *106*, 4763-4771; bJ. Zhou, X. Lin, X. Ji, S. Xu, C. Liu, X. Dong, W. Zhao, *Org. Lett.* **2020**, *22*, 4413-4417.
- [15] https://biotium.com/product/lipidspot-488-lipid-droplet-stain-1000x/?attribute_pa_dye=lipidspot-610.
- [16] C. Würth, M. Grabolle, J. Pauli, M. Spieles, U. Resch-Genger, *Nature protocols* **2013**, *8*, 1535-1550.
- [17] X. Zhang, L. Yuan, J. Jiang, J. Hu, A. du Rietz, H. Cao, R. Zhang, X. Tian, F. Zhang, Y. Ma, Z. Zhang, K. Uvdal, Z. Hu, *Anal. Chem.* **2020**, *92*, 3613-3619.
- [18] <https://www.thermofisher.com/order/catalog/product/D3922>.
- [19] aK. H. T. Mau, D. Karimlou, D. Barneda, V. Brochard, C. Royer, B. Leeke, R. A. de Souza, M. Pailles, M. Percharde, S. Srinivas, A. Jouneau, M. Christian, V. Azuara, *Nat. Commun.* **2022**, *13*, 3861; bJ. S. Hansen, S. de Maré, H. A. Jones, O. Göransson, K. Lindkvist-Petersson, *Sci. Rep.* **2017**, *7*, 15011; cT. Montanari, M. Colitti, *Histochem. Cell Biol.* **2018**, *149*, 593-605; dE. E. Spangenburg, S. J. P. Pratt, L. M. Wohlers, R. M. Lovering, *J. Biomed. Biotech.* **2011**, *2011*, 598358.
- [20] G. R. Fulmer, A. J. M. Miller, N. H. Sherden, H. E. Gottlieb, A. Nudelman, B. M. Stoltz, J. E. Bercaw, K. I. Goldberg, *Organometallics* **2010**, *29*, 2176-2179.
- [21] Y.-H. Ho, K.-J. Wang, P.-Y. Hung, Y.-S. Cheng, J.-R. Liu, S.-T. Fung, P.-H. Liang, J.-W. Chern, C.-W. Yu, *Org. Biomol. Chem.* **2018**, *16*, 7820-7832.

Entry for the Table of Contents



Due to its turn-ON response to apolar environment, the 4-DiMe-ANI enables wash-free imaging of lipid droplets in living cells with excellent LD/cytosol signal ratio

Institute and/or researcher Twitter usernames:

[@AChevalier18](#)

[@ICSN_lab](#)